

Closing the gap to convergence of gravitoturbulence in local simulations

J. Klee^{1,*}, T. F. Illenseer¹, M. Jung², and W. J. Duschl^{1,3}

¹ Institut für Theoretische Physik und Astrophysik, Christian-Albrechts-Universität zu Kiel, Leibnizstr. 15, 24118 Kiel, Germany

² Hamburger Sternwarte, Universität Hamburg, Gojenbergsweg 112, 21029 Hamburg, Germany

³ Steward Observatory, The University of Arizona, 933 N. Cherry Ave., Tucson, AZ 85721, USA

November 12, 2021, accepted for publication in A&A

ABSTRACT

Aims. Our goal is to find a converged cooling limit for fragmentation in self-gravitating disks. This is especially interesting for the formation of planets, brown dwarfs or stars and the growth of black holes. While investigating the limit, we want to give a clear criterion for the state of convergence.

Methods. We run two-dimensional shearsheet simulations with the hydrodynamic package Fosite at high resolutions. Thereby resolution and limiters are altered. Subsequently, we investigate the spectra of important physical quantities at the length scales where fragmentation occurs. In order to avoid prompt fragmentation at high resolutions we start these simulations with a fully developed gravitoturbulent state obtained at a lower resolution.

Results. We show nearly converged results for fragmentation with a critical cooling timescale $t_{\text{crit}} \sim 10 \Omega^{-1}$. We can backtrace this claim by investigating the spectra of relevant physical variables at length scales around and below the pressure scale height. We argue that well behaved results cannot be expected if counteracting quantities are varying too much on these critical length scales, either by change of resolution or numerical method. A comparison of fragmentation behaviour with the related spectra reveals that simulations behave similar, if the spectra are converged to the length scales where self-gravity leads to instabilities. Observable deviations in the results obtained with different numerical setup are confined to scales below these critical length scales.

Key words. instabilities – hydrodynamics – protoplanetary disks – accretion, accretion disks – methods: numerical

1. Introduction

Self-gravitating disks play an import role in the field of young protoplanetary disks and AGN-disks. A disk becomes gravitationally unstable if the Toomre parameter

$$Q = \frac{\kappa c_s}{\pi G \Sigma}, \quad (1)$$

fulfils $Q < 1$ (Toomre 1964). Thereby, κ is the epicyclic frequency, which becomes the angular velocity Ω in case of a Keplerian disk, c_s is the sound speed, G the gravitational constant and Σ the surface density. The Toomre criterion is viable in a local approximation with axisymmetric potential.

Local gravitation act on a certain length-scale interval, where disturbances are allowed to grow (Toomre 1964; Lin & Pringle 1987). It is determined by the critical length scale as an upper limit $L_{\text{crit}} = G \Sigma / \Omega^2$ and the Jeans length scale $L_J = c_s^2 / G \Sigma$ as a lower limit. Thus perturbances within

$$L_J \leq L \leq L_{\text{crit}} \quad (2)$$

are amplified and could eventually lead to fragmentation. Nelson (2006) imposed numerical consequences for this and stated that the Toomre-wavelength $\lambda_T = 2 L_J \sim H$ needs to be resolved by a simulation, where $H = c_s / \Omega$ is the Keplerian scale height.

Gammie (2001) showed in his paper numerically that a slow-cooling disk settles into the gravitoturbulent state (Paczynski

1978), whereas a gravitationally unstable disk that cools fast leads to fragmentation. In the former case turbulence leads to an enhanced transport of angular momentum (Lin & Pringle 1987; Balbus & Papaloizou 1999; Duschl et al. 2000; Duschl & Britsch 2006). In the latter the gaseous disk may at least partly disintegrate if giant planets, brown dwarfs or, in case of AGN disks, even massive stars form within the disk (Rice et al. 2015; Baehr et al. 2017; Boss 1998; Levin & Beloborodov 2003). The criterion for fragmentation that Gammie (2001) ascertains is that the cooling fulfils $\beta = t_c \Omega < 3$, where β is a dimensionless quantity describing the cooling timescale t_c in terms of orbital timescale Ω^{-1} . The value for β can also be related to an effective viscosity parameter $\alpha = (\gamma(\gamma - 1) q^2 \beta)^{-1}$ (Gammie 2001; Shakura & Sunyaev 1973). Here, γ is the ratio of specific heat capacities and $q = -\frac{\partial \ln \Omega}{\partial \ln r}$ is the power-law exponent of the rotation law which becomes 3/2 for Keplerian motion.

However, simulations show also fragmentation for larger β , while going to higher resolutions (Meru & Bate 2011; Paardekooper et al. 2011). This non-convergence also takes place in the local-approximation (Paardekooper 2012; Baehr & Klahr 2015; Klee et al. 2017). Even by using an altered cooling at small scales, Baehr & Klahr (2015) suffer from fragmentation in their high-resolution runs. Recently, Deng et al. (2017) show that codes that rely on smoothed particle hydrodynamics that use artificial viscosity also have problems with artificial fragmentation. This can be circumvented by using meshless methods. But also grid based codes with shock capturing mechanisms can get

* jklee@astrophysik.uni-kiel.de

into troubles, where limiting functions can have a strong impact on the outcome of the simulations Klee et al. (2017).

(Young & Clarke 2015) also observed fragmentation above the critical β_{crit} in their simulations. They proposed that a quasi-static collapse can explain this behaviour. Paardekooper (2012) shows that there is also a stochastic component when running over long timescales.

More recently, also three dimensional shearingbox simulations were carried out in the local approximation (Shi & Chiang 2014). Baehr et al. (2017) found fragmentation at around $\beta \lesssim 3$ reaching high resolutions with very small box-sizes. Riols et al. (2017) show that at sufficiently high resolutions small scale turbulences set in, off the midplane. They furthermore point out that the energy spectrum of gravitoturbulence can be approximated by the $k^{-5/3}$ cascade (Kolmogorov 1941). However, they raise the problem already revealed by (Gammie 2001) that in order to have a well-behaved gravitoturbulent state the box size should be not too small. They conclude a box size of at least $\gtrsim 40 H = 40\pi L_{\text{crit}}$. Otherwise bursts that might be connected to transient fragmentation set in. Booth & Clarke (2018) propose a minimal size of the shearingbox $\gtrsim 64 H$ in horizontal direction. Otherwise long term trends show up.

In this paper we investigate fragmentation at very high horizontal resolutions while preserving a well-behaved gravitoturbulent state in a sufficiently large shearing sheet. We first describe our methods in section 2, explaining the underlying equations and the setup. In section 3 we present the numerical results obtained for highest resolutions and closed to converged spectra for various quantities. Finally, we discuss and conclude on our results in section 4.

2. Methods

We use the hydrodynamic code *Fosite* by Illenseer & Duschl (2009), a generalized version of the finite volume method of Kurganov & Tadmor (2000). *Fosite* can operate on arbitrary curvilinear-orthogonal grids and is fully parallelized and vectorized. It uses modern Fortran 2008 language features and object-oriented design patterns. *Fosite* has recently been ported and optimized for the new NEC SX-Aurora Tsubasa vector computer which gave us the ability to carry out simulations with unprecedented high resolution in two dimensions¹.

2.1. Hydrodynamic Equations

We solve the two-dimensional hydrodynamical equations in the local approximation (Goldreich & Lynden-Bell 1965; Hawley et al. 1995). Together with the Poisson equation for a razor thin disk (Gammie 2001) the system of equations is

$$\frac{\partial \Sigma}{\partial t} + \nabla \cdot (\Sigma \mathbf{v}) - q\Omega y \frac{\partial \Sigma}{\partial x} = 0, \quad (3a)$$

$$\frac{\partial \Sigma \mathbf{v}}{\partial t} + \nabla \cdot (\Sigma \mathbf{v} \otimes \mathbf{v} + p \mathbb{I}) - q\Omega y \frac{\partial \Sigma \mathbf{v}}{\partial x} = \Omega \Sigma \begin{pmatrix} (2-q)v_y \\ -2v_x \end{pmatrix} - \Sigma \nabla \Phi_{\text{sg}}, \quad (3b)$$

$$\begin{aligned} \frac{\partial E}{\partial t} + \nabla \cdot ((E+p) \mathbf{v}) - q\Omega y \frac{\partial E}{\partial x} = & -q\Omega \Sigma v_x v_y \\ & - \Sigma \nabla \Phi_{\text{sg}} \cdot \mathbf{v} - \Sigma Q_{\text{cool}}, \end{aligned} \quad (3c)$$

$$\Delta \Phi_{\text{sg}} = 4\pi G \Sigma \delta(z). \quad (3d)$$

¹ The code is freely available under <https://github.com/tillense/fosite>.

Here, p is the integrated pressure and $\mathbf{v} = v_x \hat{\mathbf{e}}_x + v_y \hat{\mathbf{e}}_y$ is the residual part of the two dimensional velocity, by splitting of a background velocity $q\Omega y \hat{\mathbf{e}}_x$. The according total energy is $E = \frac{1}{2} m |\mathbf{v}|^2 + p/(\gamma - 1)$. The additional advection step, which is the last term on the left hand side of eqs. 3a - 3c is calculated separately in order to allow for very large time steps (Masset 2000; Jung et al. 2018). The gravitational potential of the shearing-sheet Φ_{sg} describes the self-gravitation. Thereby, $\delta(z)$ is the delta-distribution. The according Poisson equation 3d is solved in Fourier space (Gammie 2001; Klee et al. 2017), imposing periodic boundary conditions. This is achieved by shifting the whole density field to the next periodic point before applying the transformation (Gammie 2001; Klee et al. 2017). Finally, $Q_{\text{cool}} = \frac{p\Omega}{(\gamma-1)\beta}$ is the well-known cooling parametrization (Gammie 2001).

2.2. Numerical Setup

In order to have a well-tuned setup we rely on the results in Klee et al. (2017). There different numerical shock-capturing mechanisms (limiting functions) are tested against each other. We thus prefer van-Leer limiting (van Leer 1974), which showed to be advantageous in contrast to other limiting functions, regarding artificial fragmentation. However, most simulations were again carried out using the Superbee limiter (Roe & Baines 1982) for comparison. Additionally, we use Dormand-Prince time stepping (Dormand & Prince 1980), which showed the best results in the epicyclic motion test (Klee et al. 2017).

We rotate the computational domain by 90° in contrast to Klee et al. (2017). This is advantageous in order to have the first dimension completely accessible for the parallel Fourier solver, while preserving vectorization. We thus decomposed the grid in pencils along the y -direction.

2.2.1. Simulation setup

With $L_x = L_y = 320 L_{\text{crit}}$ we use the same grid size as in Gammie (2001). This corresponds to $\sim 100 H$. It ensures that we are not getting into trouble with long-term periodics as stated in Booth & Clarke (2018). Another reason for staying with a relatively large extent of the box compared to other three-dimensional simulations is already given by Gammie (2001, Fig. 9). There, the contribution of the gravitational component of the stress is taken into consideration for twice of our size $L = 640 L_{\text{crit}}$. Taking the length of $L = 320 L_{\text{crit}}$ into account, still includes $\sim 90\%$ of the gravitational component. Further reduction of box size removes a significant amount of gravitational stress from the simulations which may have a major impact on the results. This is supported by the observations of Riols et al. (2017) and Booth & Clarke (2018) who found that whereas some parameters, like Toomre's Q converge quite fast for increasing box sizes, kinetic energy and gravitational stress are not doing so.

We use $\gamma = 2.0$ in order to conform to previous results Gammie (2001); Paardekooper (2012); Klee et al. (2017). It should be kept in mind, however, that smaller γ generally increase the probability for fragmentation (Rice 2016).

Booth & Clarke (2018) investigated in more detail the problem of prompt fragmentation, where fragments form during initialization. In Klee et al. (2017) we already used the approach of slowly moving down the cooling in order to prevent this kind of fragmentation also in local simulations. However, going to higher resolutions made it increasingly harder for us to prevent the artificial fragmentation in this manner. Additionally, reaching

the gravitoturbulent state needs more and more time, for higher resolutions and slower (initial) cooling.

In this work, we take another approach. Instead of fine-tuning the initial cooling, we reuse the result of a previous fully developed low resolution run with slow cooling using spline-interpolation to generate high resolution data². Thereby we already initiate the high resolution simulation with a gravitoturbulent state. This approach also saves a significant amount of computational time skipping the initial phase in which the simulation settles into the gravitoturbulent state.

3. Simulations and results

Table 1. Overview of simulation runs

Name	Lim.	Res.	β	$T_{\text{sim}} \Omega$	Frag.
VL4096B5	VL	4096	5	50	Yes
VL4096B7-5	VL	4096	7.5	175	Yes
VL4096B10	VL	4096	10.0	200	Yes
VL4096B15	VL	4096	15.0	200	No
VL4096B20	VL	4096	20.0	200	No
VL8192B5	VL	8192	5.0	34	Yes
VL8192B10	VL	8192	10.0	120	Yes
VL8192B15	VL	8192	15.0	120	No
VL8192B20	VL	8192	20.0	100	No
SB4096B5	SB	4096	5	50	Yes
SB4096B7-5	SB	4096	7.5	100	Yes
SB4096B10	SB	4096	10.0	250	Yes
SB4096B15	SB	4096	15.0	200	No
SB4096B20	SB	4096	20.0	200	No
SB8192B5	SB	8192	5.0	100	Yes
SB8192B7-5	SB	8192	7.5	50	Yes
SB8192B10	SB	8192	10.0	100	No

Notes. VL - van-Leer, SB - Superbee, T_{sim} - simulation time

Table 1 shows an overview of the simulations that were done. We ran simulations at twice and four times the highest resolution in Klee et al. (2017), which corresponds to a resolution of 4096 and 8192, respectively.

As initial conditions for the runs with resolution 4096, we used a gravitoturbulent run with a resolution of 2048, van-Leer limiting and $\beta = 10$. Since our run at $\beta = 10$ fragmented at a resolution of 4096 we used the run with $\beta = 15$ as a starting point for the runs with a resolution of 8192. At a resolution of 4096 the normal runtime is $200 \Omega^{-1}$ and at 8192 it is $100 \Omega^{-1}$. If many clear fragments formed we stopped the run earlier. For small density enhancements at the end of the run we optionally extended the run to investigate its outcome.

In case of simulations carried out with the Superbee limiter, a close inspection of the region within $y = \pm 20 L_{\text{crit}}$ reveals small almost circular features with unusual density depletion which were never observed in simulations with van-Leer limiter. It is not clear to us what determines the spatial occurrence and extent as well as the life time of these structures. As a matter of fact they seem to be continuously generated only around the mid-plane with scales of the order of at most a few L_{crit} and are therefore only visible in the simulations at resolutions 4096 and 8192. If they encounter strong shocks they are often completely destroyed but some of them survive for several orbital time scales.

² RegularGridInterpolator of the SciPy package (Jones et al. 2001–2019).

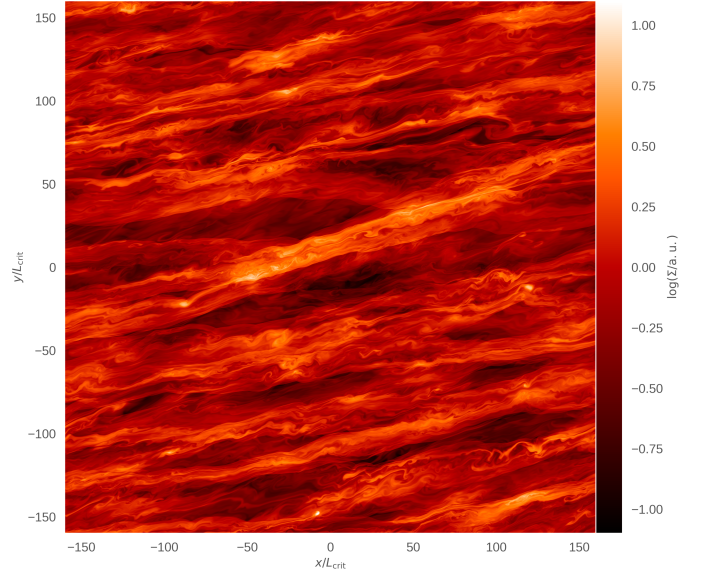


Fig. 1. Snapshot of the surface density of the gravitoturbulent state at a resolution of 8192 for $\beta = 10$ and van-Leer limiting. This simulation shows later fragments with 20 – 30 times the background density.

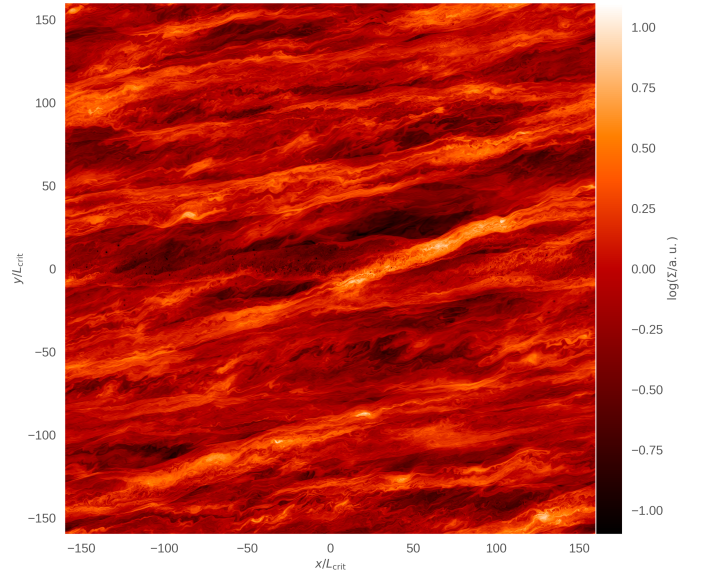


Fig. 2. Snapshot of the surface density of the gravitoturbulent state at a resolution of 8192 for $\beta = 10$ and Superbee limiting.

We think that these structures are numerical artifacts again caused by oversteepening (Klee et al. 2017). Since the Superbee limiter tends to overestimate spatial gradients it amplifies low-pressure areas. The results shown for the isentropic vortex test Yee et al. (1999) in App. A support this hypothesis. They clearly illustrate that the Superbee limiter enhances the central pressure trough while the van-Leer limiter depletes it.

Fig. 1, 2 and 3 show snapshots of the high-resolution results obtained with different limiters and cooling parameters. In case of the gravitoturbulent simulations we also provide movies for better illustration of what is going on in these simulations and to make the differences between the two limiters clearer.

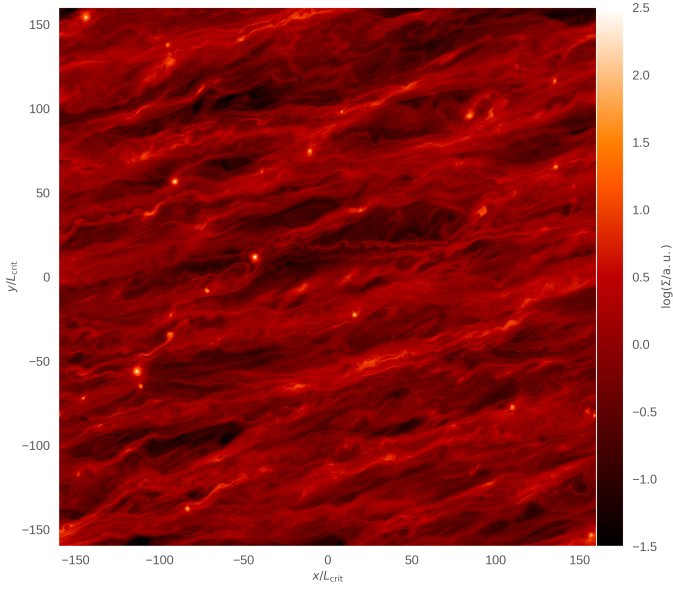


Fig. 3. Snapshot of the surface density in a fully fragmented run at a resolution of 8192 for $\beta = 5$ and van-Leer limiting.

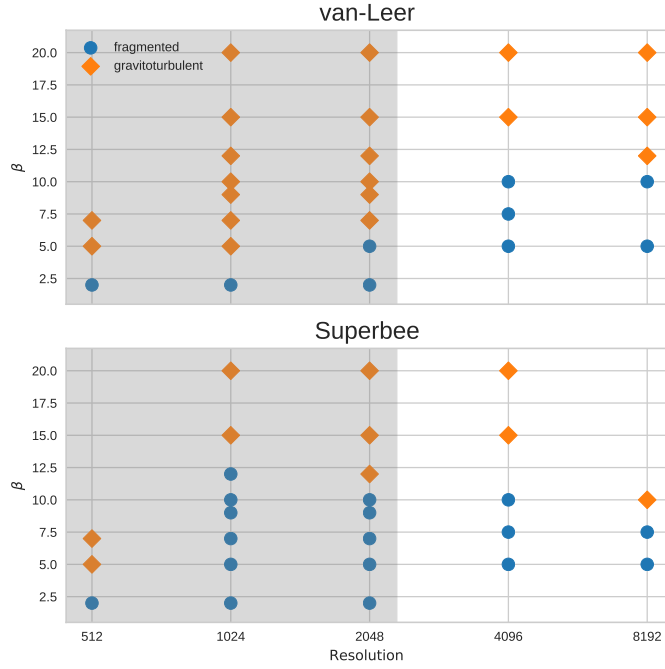


Fig. 4. Fragmentation plot for different resolutions N and cooling timescales β . The gray regions show results already published in Klee et al. (2017). The simulations seem to converge at the highest resolutions to a value of $\beta_{\text{crit}} \approx 10$ for both numerical schemes.

3.1. Fragmentation

Fig. 4 summarizes which simulations showed fragmentation. Besides the new runs we also added the results for lower resolutions from Klee et al. (2017). For higher resolutions the question whether or not fragmentation occurs is less affected by the limiter. This is not what we would expect in view of our argumentation in Klee et al. (2017), where Superbee suffers from numerical errors that force fragmentation. Looking at even higher resolutions, we see that the Superbee limiter does not fragment for $\beta = 10$. Thus in contrast to our previous findings it seems

that the Superbee limiter yields similar results with respect to the fragmenting behaviour and the threshold for fragmentation stabilizes around $\beta \sim 10$.

For $\beta = 10$ and van-Leer limiting at $N = 4096$ we have a single fragment that forms between $50 \Omega^{-1}$ and $75 \Omega^{-1}$ and is disrupted again before the end of the run. On the other side we had a fragment for the same setup with Superbee at the regular end of the simulation. We then extended the simulation another $50 \Omega^{-1}$ in order to ensure that it is stable for a longer period. A similar behaviour was found in the run with $N = 8192$ for van-Leer limiting and $\beta = 10$. In this case a fragment forms around $\sim 80 \Omega^{-1}$ which has 20 – 30 times the background density and is stable for at least $\sim 40 \Omega^{-1}$. Thus only single or few fragments form in the range $5 < \beta \lesssim 10$ whereas below $\beta = 5$ the whole field fragments immediately (cf. Fig. 3). In addition, if $\beta \sim 10$ these single fragments do sometimes not survive for longer periods. Therefore the conclusion whether or not the simulation is fragmented seems less clear in these cases since it depends on the formation and stability of a single fragment.

3.2. Convergence of spectra at important length scales

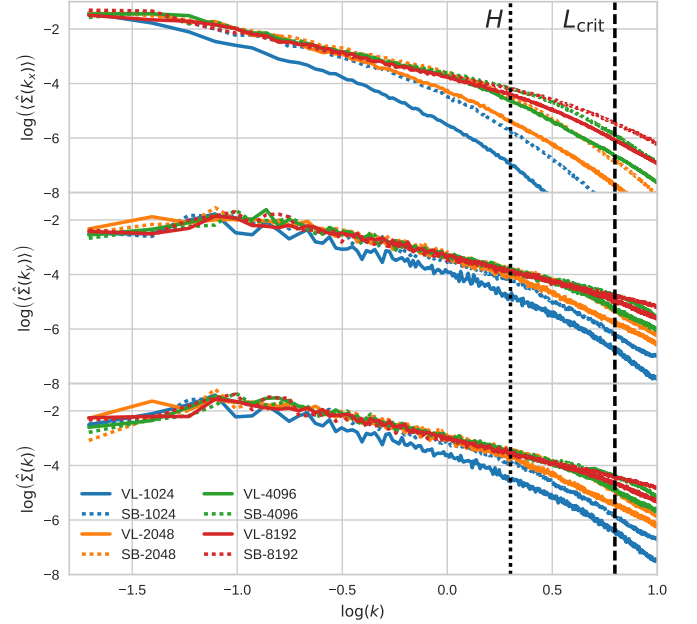


Fig. 5. Components of the density spectrum for different resolutions and limiters. The density spectrum is well converged at highest resolutions to a length scale of H . The component in x -direction is only close to convergence down to L_{crit} .

In Fig. 5 and Fig. 6 we show density and pressure spectra, respectively. The spectra are adopted for a cooling parameter of $\beta = 10$ at a state where fragmentation did not occur, yet (if present). Thereby, their components in k_x , k_y and k are displayed. We see most pronounced in the surface density that the results obtained with low resolutions deviate significantly from those at higher resolutions even on length scales of the order of the scale height and above. The plots show that runs at the same resolution but with different limiters can lead to a deviation in the spectra that is partially larger than an order of magnitude. The difference between resolutions is here of several magnitudes. At higher resolutions we see that the spectral quantities are very similar and follow the cascade down to the scale height H . For many quanti-

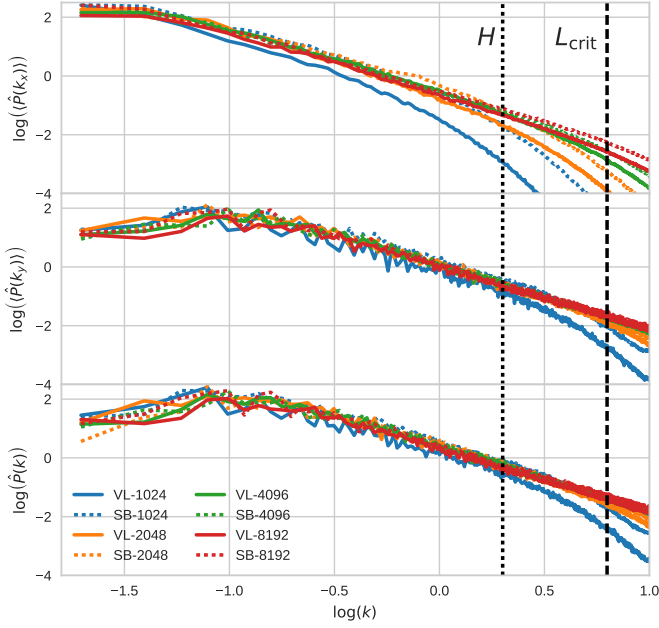


Fig. 6. Components of the pressure spectrum for different resolutions and limiters. The pressure spectrum is well converged at highest resolutions even to a length scale of L_{crit} .

ties this is even true for the smaller length scale L_{crit} , especially at the resolution of 8192. The x -components, which correspond in our case to the direction which is more parallel to the shock fronts, lacks a bit of convergence at least at the length-scale L_{crit} .

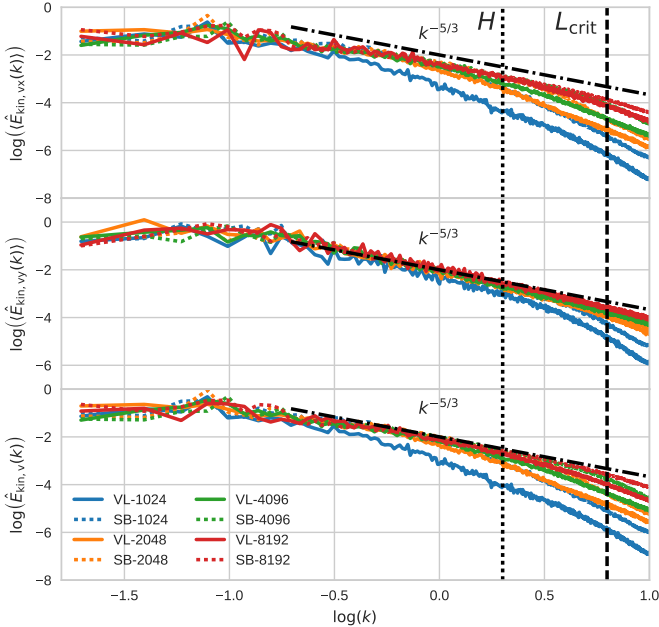


Fig. 7. Spectrum of kinetic energy for different resolutions and limiters. The velocities are summed in Fourier space along the radius k . The spectrum fulfils the $k^{-5/3}$ well at highest resolution down to L_{crit} .

In Fig. 7 we show spectra of the kinetic energy. In contrast to Fig. 5 and 6 we do not show the components along k_x or k_y but the kinetic energy associated with v_x , v_y and $|\mathbf{v}|$, always summed up along the radius in Fourier space k . We see in Fig. 7 the $k^{-5/3}$ -law fairly good, which is expected in two dimensions at large scales (Kraichnan 1967).

All figures mentioned above show well-converged spectra at the scale height H at high resolutions. Additionally, they even have few differences at L_{crit} . Having a look again at Fig. 4 we can state that the simulations that show differences with respect to fragmenting behaviour also show differences for the physical quantities at the length scales where fragmentation occurs.

When this gap is closed, we also see smaller differences in the fragmenting behaviour. We thus have a clear criterion for convergence, which does not only rely on the observation of forming clumps, but on the turbulent cascade down to the relevant length scales.

4. Discussion & Conclusion

We show results of self-gravitating shearing sheet simulations conducted in two dimensions at the highest resolution so far and investigate the fragmentation behaviour. In order to overcome prompt fragmentation we interpolate from an already evolved gravitoturbulent state with lower resolutions and use this as initial conditions. However, even then we get a relatively large critical value of $\beta_{\text{crit}} \lesssim 10$ as a fragmentation criterion. We regard this result as robust and independent of resolution as long as it exceeds 4096 at the least (40 cell per scale-height H). Still, there seems to be some uncertainty around the aforementioned β_{crit} swiftly declining for higher values. This holds also for different numerical schemes within the code, where we know that one of the limiting functions is prone to numerical errors. However, even with these errors the critical value β_{crit} is not affected too much.

That is why we think that we are close to convergence. As a definition for that state we do not only have a look at the fragmentation behaviour with ever higher resolutions. Instead we investigate physical quantities of interest at the length scales where fragmentation occurs. When resolutions are high enough, the small scale structures show very clear cascades down to the length-scales of interest in eq. 2. Although even smaller structures can vary fundamentally between the numerical schemes, we get similar results for fragmentation. We conclude that the differences in the smallest structures have (nearly) no influence on the fragmentation process. This is the case, because the amplified modes by self-gravity only affect the length scales in eq. 2.

Recent results preferred a clearer criterion at around $\beta_{\text{crit}} = 3$ (Baehr et al. 2017; Booth & Clarke 2018; Deng et al. 2017). They all have the advantage that they were run in three dimensions. However, in order to reach the necessary high horizontal resolutions Baehr et al. (2017) and Booth & Clarke (2018) reduce the spatial dimensions ($12H$ and max. $32H$) for the runs in which they investigate fragmentation. Indeed we see that the runs where Booth & Clarke (2018) resolve H by 32 grid cells show fragmentation for slightly larger $\beta_{\text{crit}} \sim 4$. Interestingly, this corresponds to our runs between resolutions of 2048 and 4096 (cf. Fig. 4). Deng et al. (2017) also show that they see no fragmentation at higher resolutions with the meshless method code Gizmo (Hopkins 2014). They state this is due to the lack of artificial viscosity in these schemes. However, their code introduces slope limiting procedures, similar to those used in our code Fosite which evidentially impact the outcome of fragmentation studies (Klee et al. 2017).

It should also be taken into account, that two-dimensional turbulence can behave differently when compared to three-dimensional turbulence. It has an additional turbulent energy

cascade at small scales with $\propto k^{-3}$ (Kraichnan 1967; Boffetta & Ecke 2012; Kolmogorov 1941). We see a fairly clear $k^{-5/3}$ cascade down to L_{crit} (cf. Fig. 7). On scales below L_{crit} , however, the flow is no longer turbulent, because gravitational instabilities are not amplified anymore. Nevertheless, it would be interesting to carry out a similar analysis of converged spectra in three-dimensional simulations and verify these considerations.

The larger value of β_{crit} has some implications for fragmenting disks. Relating the critical cooling parameter to the effective viscosity parameter α yields a smaller critical value for this number around $\alpha_{\text{crit}} \sim 0.02$ Gammie (2001). This would indeed mean that α -parametrizations with larger values might not be well-suited in case of self-gravitating disks.

This reasoning becomes less clear if one takes additional heat sources into account. For example, Rice et al. (2011) show that an additional background irradiation cannot suppress fragmentation, but leads to fragmentation at smaller β_{crit} with smaller values for α_{crit} . The former direct relation between the two parameters is then disconnected. Even when the cooling is fast, the reachable value for α_{crit} becomes smaller.

In case of protoplanetary disks the shift to a larger value of β_{crit} has not necessarily a strong impact on the radial distance for fragmentation in a global setup. Generally, for larger β_{crit} fragmentation can occur closer to the central object with a relation of $\beta \propto r^{-9/2}$ (Clarke & Lodato 2009). The cooling parameter thus strongly depends on the radius (Paardekooper 2012), which leads to little effect in radial change. The distance of formation would than still be at a radius of some ten astronomical units (Meru & Bate 2012). Regarding the lifetime of self-gravitating protoplanetary disks of $\sim 10^5$ yr (Laughlin & Bodenheimer 1994; Haisch Jr et al. 2001) the results are still relevant. Taking into consideration a radius of $r = 100$ au the disk would survive for ~ 100 orbits whereas the simulations of this work were done for up to $200 \Omega^{-1}$ which would account for ~ 32 orbits.

Finally, we come to the conclusion that while going to ever higher resolution we inevitably see again a shift to a larger $\beta_{\text{crit}} \sim 10$ with some uncertainty around that value. While for $\beta \lesssim 5$ the whole field fragments, we see only single or a few fragments around $5 < \beta \lesssim 10$. Because of the close to converged spectra with different numerical setups we do not expect this upper limit to change too much anymore.

Acknowledgements. We thank the anonymous referee for the very helpful comments and suggestions on a more recent version of this publication.

References

Baehr, H. & Klahr, H. 2015, *The Astrophysical Journal*, 814, 155
 Baehr, H., Klahr, H., & Kratter, K. M. 2017, *The Astrophysical Journal*, 848, 40
 Balbus, S. A. & Papaloizou, J. C. 1999, *The Astrophysical Journal*, 521, 650
 Boffetta, G. & Ecke, R. E. 2012, *Annual Review of Fluid Mechanics*, 44, 427
 Booth, R. A. & Clarke, C. J. 2018, *Monthly Notices of the Royal Astronomical Society*, 483, 3718
 Boss, A. P. 1998, *The Astrophysical Journal*, 503, 923
 Clarke, C. & Lodato, G. 2009, *Monthly Notices of the Royal Astronomical Society: Letters*, 398, L6
 Deng, H., Mayer, L., & Meru, F. 2017, *The Astrophysical Journal*, 847, 43
 Dormand, J. R. & Prince, P. J. 1980, *Journal of computational and applied mathematics*, 6, 19
 Duschl, W. J. & Britsch, M. 2006, *The Astrophysical Journal Letters*, 653, L89
 Duschl, W. J., Strittmatter, P. A., & Biermann, P. L. 2000, *A&A*, 357, 1123
 Gammie, C. F. 2001, *The Astrophysical Journal*, 553, 174
 Goldreich, P. & Lynden-Bell, D. 1965, *Monthly Notices of the Royal Astronomical Society*, 130, 125
 Haisch Jr, K. E., Lada, E. A., & Lada, C. J. 2001, *The Astrophysical Journal Letters*, 553, L153

Hawley, J. F., Gammie, C. F., & Balbus, S. A. 1995, *The Astrophysical Journal*, 440, 742
 Hopkins, P. F. 2014, *Astrophysics Source Code Library*
 Illenseer, T. F. & Duschl, W. J. 2009, *Computer Physics Communications*, 180, 2283
 Jones, E., Oliphant, T., Peterson, P., et al. 2001–2019, *SciPy: Open source scientific tools for Python*, [Online; accessed February 20, 2019]
 Jung, M., Illenseer, T. F., & Duschl, W. J. 2018, *arXiv preprint arXiv:1803.02055*
 Klee, J., Illenseer, T. F., Jung, M., & Duschl, W. J. 2017, *Astronomy & Astrophysics*, 606, A70
 Kolmogorov, A. N. 1941, *Cr Acad. Sci. URSS*, 30, 301
 Kraichnan, R. H. 1967, *The Physics of Fluids*, 10, 1417
 Kurganov, A. & Tadmor, E. 2000, *Journal of Computational Physics*, 160, 241
 Laughlin, G. & Bodenheimer, P. 1994, *The Astrophysical Journal*, 436, 335
 Levin, Y. & Beloborodov, A. M. 2003, *The Astrophysical Journal Letters*, 590, L33
 Lin, D. & Pringle, J. 1987, *Monthly Notices of the Royal Astronomical Society*, 225, 607
 Masset, F. 2000, *Astronomy and Astrophysics Supplement Series*, 141, 165
 Meru, F. & Bate, M. R. 2011, *Monthly Notices of the Royal Astronomical Society: Letters*, 411, L1
 Meru, F. & Bate, M. R. 2012, *Monthly Notices of the Royal Astronomical Society*, 427, 2022
 Nelson, A. F. 2006, *Monthly Notices of the Royal Astronomical Society*, 373, 1039
 Paardekooper, S.-J. 2012, *Monthly Notices of the Royal Astronomical Society*, 421, 3286
 Paardekooper, S.-J., Baruteau, C., & Meru, F. 2011, *Monthly Notices of the Royal Astronomical Society: Letters*, 416, L65
 Paczynski, B. 1978, *Acta Astronomica*, 28, 91
 Rice, K. 2016, *Publications of the Astronomical Society of Australia*, 33
 Rice, K., Lopez, E., Forgan, D., & Biller, B. 2015, *Monthly Notices of the Royal Astronomical Society*, 454, 1940
 Rice, W., Armitage, P., Mamatsashvili, G., Lodato, G., & Clarke, C. 2011, *Monthly Notices of the Royal Astronomical Society*, 418, 1356
 Riols, A., Latter, H., & Paardekooper, S.-J. 2017, *Monthly Notices of the Royal Astronomical Society*, 471, 317
 Roe, P. L. & Baines, M. J. 1982, 281–290
 Shakura, N. I. & Sunyaev, R. A. 1973, *Astronomy and Astrophysics*, 24, 337
 Shi, J.-M. & Chiang, E. 2014, *The Astrophysical Journal*, 789, 34
 Toomre, A. 1964, *The Astrophysical Journal*, 139, 1217
 van Leer, B. 1974, *Journal of Computational Physics*, 14, 361
 Yee, H. C., Sandham, N. D., & Djomehri, M. J. 1999, *Journal of computational physics*, 150, 199
 Young, M. D. & Clarke, C. J. 2015, *Monthly Notices of the Royal Astronomical Society*, 451, 3987

Appendix A: Vortex Test Cuts

In Fig. A.1 cuts of isentropic vortex tests are presented. The setup is described in (Yee et al. 1999; Jung et al. 2018). It has initial conditions

$$\varrho = \varrho_\infty \left(1 - \frac{(\gamma - 1)}{8\gamma\pi^2} e^{1-r^2} \right)^{\frac{1}{\gamma-1}} \quad (\text{A.1})$$

$$v_x = \left(1 - \frac{\chi}{2\pi} e^{\frac{1-r^2}{2}} \right) \quad (\text{A.2})$$

$$v_y = \left(1 + \frac{\chi}{2\pi} e^{\frac{1-r^2}{2}} \right) \quad (\text{A.3})$$

$$p = p_\infty \left(\frac{\varrho}{\varrho_\infty} \right)^\gamma, \quad (\text{A.4})$$

with density ϱ , pressure p and v_x , v_y velocities in the according directions. $r = \sqrt{x^2 + y^2}$ is the distance from the center of the vortex. The other setup parameters are summarized in Table A.1. The results with van-Leer and Superbee limiting show a qualita-

Table A.1. Setup for isentropic vortex

setup variable	numerical value
background density ϱ_∞	1.0
background pressure p_∞	1.0
vortex strength χ	5.0
adiabatic index γ	1.4
domain size $x \times y$	$[-5, 5] \times [-5, 5]$
resolution $N_x \times N_y$	40×40
limiters	van-Leer, Superbee
simulation time T	30

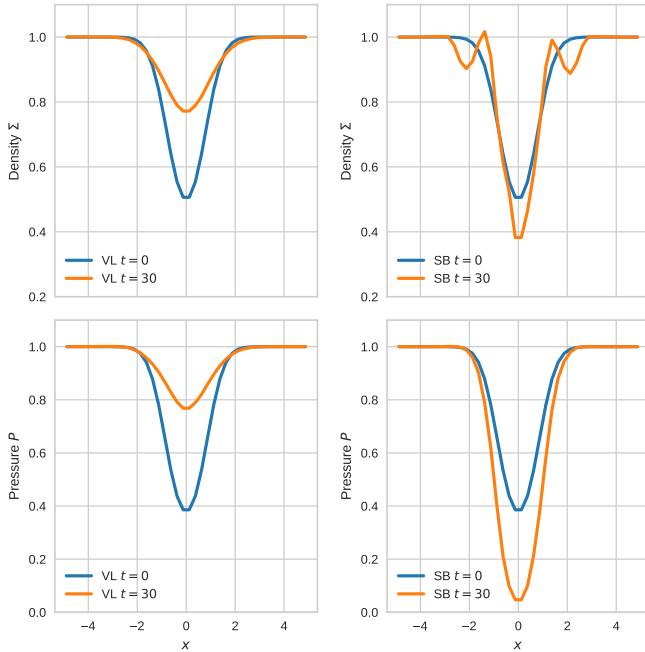


Fig. A.1. Cuts along the x -axis at $y = 0.0$ for an isentropic vortex on a cartesian grid. *Left (van-Leer)*: density and pressure are smeared out. *Right (Superbee)*: density and pressure are both oversteepened with time.

tive difference regarding the evolution. With van-Leer the vortex is smeared out, while with Superbee the vortex is strengthened.